Mon. Not. R. Astron. Soc. **326,** 333–341 (2001)

Deep colour–magnitude diagrams of LMC field stars imaged with *HST*

R. Castro,[1] B. X. Santiago,[1★] G. F. Gilmore,[2] S. Beaulieu[2] and R. A. Johnson[2]
[1]*Universidade Federal do Rio Grande do Sul, Instituto de Física, 91501-970 Porto Alegre, RS Brasil*
[2]*Institute of Astronomy, Madingley Road, Cambridge CB3 0HA*

Accepted 2001 April 19. Received 2001 March 12; in original form 2000 August 30

ABSTRACT

We present deep photometry ($V \lesssim 26$) in V and I bands obtained with the Wide Field and Planetary Camera 2 on board the *Hubble Space Telescope* for 7 fields $\sim 5°$ away from the Large Magellanic Cloud centre. The fields contain, typically, 2000 stars each. Isochrones were fitted to the colour–magnitude diagrams in order to identify different star populations in these fields. An old population ($\tau > 10$ Gyr) has been found in all fields. Some events of enhanced star formation, with ages between 2 and 4 Gyr, were identified in the fields localized in the north to north-west regions. Luminosity functions of low-mass stars were also obtained for all fields. Kolmogorov Smirnov test results suggest differences smaller than 30 per cent in the mixture of stellar populations contributing to the fields. Finally, density profiles were derived for old and intermediate-age stars. The former shows a slightly steeper decline than the latter.

Key words: stars: statistics – galaxies: evolution – galaxies: structure.

1 INTRODUCTION

Even with the highest-resolution instruments, it is not yet possible to resolve individual stars in images of distant galaxies. Therefore, our Milky Way galaxy and its closest neighbours in the Local Group remain the main source of information about stellar populations. Knowledge about the present stellar content within nearby galaxies of different types, besides being an essential step towards recovering their star formation history and understanding their evolution, is a powerful tool in interpreting integrated images and spectra of distant galaxies.

The Magellanic Clouds, and in particular the Large Magellanic Cloud (LMC), have been increasingly targeted in studies of stellar populations, given their proximity to the Galaxy and their markedly distinct properties. Many studies have concentrated on the extensive cluster system in the LMC, displaying a wide range of ages and properties, but for which there seems to be an age gap, with essentially no clusters with ages in the range $4 \lesssim \tau \lesssim 10$ Gyr (Jensen, Mould & Reid 1988; Da Costa 1991). As for their spatial and kinematical distribution, LMC clusters seem to make up a rotating disc, regardless of age (Schommer et al. 1992; Olszewski 1993).

Field stars are probably more representative of the overall star formation history in the LMC. The complexity of analysing colour–magnitude diagrams (CMDs) with heterogeneous mixtures of populations, and the need for deep high-resolution photometry in order to explore the turn-off points of old and intermediate-age populations, have been the main obstacles to analyses of field stellar samples (Olszewski, Suntzeff & Mateo 1996). Ground-based studies have concluded that the bulk of star formation has occurred in the past 4 Gyr. Bertelli et al. (1992) suggest a constant star formation rate (SFR) in the LMC during the past 4 Gyr, with an order of magnitude decrease in SFR at earlier times. Similar conclusions have resulted from the analyses by Westerlund, Linde & Lynga (1995) and Vallenari et al. (1996). These latter authors identify events of enhanced star formation at 2.0, 2.5 and 4.0 Gyr in different LMC fields. More recently, work has been based on *Hubble Space Telescope* (*HST*) data. Gallagher et al. (1996) have suggested a roughly constant SFR in the past few Gyr, except for a small period of enhanced star formation about 2 Gyr ago. Holtzman et al. (1997) analysed the luminosity function of stars in the same *HST* field, located some 4° from the LMC bar, and favoured a constant SFR for 10 Gyr in the LMC followed by a factor of 3 increase in the last 2 Gyr, yielding roughly the same number of stars younger and older than 4 Gyr. They also identified an intermediate-age turn-off in their field. Elson, Gilmore & Santiago (1997) have studied an *HST* field closer to the LMC bar and have identified two main populations, with ages $\tau \sim 1$–2 Gyr and $\tau \sim 2$–4 Gyr, the exact ages depending on metallicity. Geha et al. (1998) have studied three *HST* fields in the outer region of the LMC and also favour a model with roughly equal numbers of stars younger and older than $\tau = 4$ Gyr.

In this paper we analyze seven fields imaged with *HST*'s Wide Field and Planetary Camera (WFPC2) in two filters and situated in different directions within the LMC, at angular distances varying from $\sim 4°$ to $\sim 6°$ from its centre. The fields were observed in parallel to NICMOS and STIS exposures of rich clusters targeted by the 'Formation and evolution of rich LMC clusters' project

★E-mail: santiago@if.ufrgs.br (BXS)

(LMC7307) (Beaulieu et al. 1998; Elson et al. 1998a,b; Johnson et al. 1998). Our main goals are the identification of individual populations from the observed CMDs, determination of ages and metallicities (especially for the oldest field stars in the LMC), and analysis of possible variations in population mix from one region of the LMC to the other. In Section 2 we present the data, describing the field characteristics and exposure times, sample selection and photometry. The CMDs are presented in Section 3 along with isochrone fits using modern grids. In Section 4 we compare the stellar luminosity functions (LFs) of different fields in an attempt to discuss the population mix and its possible variations. Density profiles of different populations within our limited angular range are also shown. Finally, in Section 5 we present our conclusions.

Table 1. Fields description. The columns list the field ID, right ascension and declination, angular distance to the LMC centre, and the date when they were observed. Notice that the fields are identified by the rich cluster with which they were observed in parallel.

Field ID	α(2000)	δ(2000)	Ang. Dist. (°)	Date
Hodge 11	6 15 43	−69 48 18	4.5	1998 April 20
Hodge 14	5 28 50	−73 30 32	3.8	1998 February 4
NGC1805	5 01 28	−66 01 43	4.3	1997 December 8
NGC1818	5 03 24	−66 20 42	3.9	1997 December 11
NGC1831	5 05 34	−64 49 17	5.2	1997 December 18
NGC1868	5 15 31	−63 53 07	5.9	1998 March 23
NGC2209	6 09 58	−73 45 40	5.4	1998 March 31

Table 2. The columns show: field ID, cluster visual radius and redenning, adopted distance modulus and total number of stars.

Field	Cluster radius	$E(B-V)$	Dist. Mod.	# of stars
Hodge 11	1.4′	0.0	18.34	2056
Hodge 14	1.2′	0.04	18.49	2816
NGC1805	0.8′	0.04	18.59	3798
NGC1818	1.3′	0.03	18.58	4887
NGC1831	1.2′	0.0	18.58	2030
NGC1868	1.4′	0.02	18.55	1699
NGC2209	1.2′	0.07	18.39	1314

2 OBSERVATIONS

The seven *HST*/WFPC2 fields analysed in this work were imaged with two filters: F555W and F814W, closely matching Johnson–Cousins *V* and *I*, respectively. The total exposure times were 1200s for F555W and 800s for F814W. Two exposures were taken with each filter in order to facilitate cosmic-ray subtraction. Saturation limits are of about $V_{555} \simeq 18.5$ and $I_{814} \simeq 17.5$.

Table 1 lists the field IDs, borrowed from the rich clusters close to which they lie, their equatorial coordinates for the 2000 epoch, their angular distance from the optical LMC centre (this last taken from Westerlund 1990) and the date of the observations.

Table 2 shows more information related to the fields. It lists the visual radius of the rich clusters, taken from their density profiles (Santiago et al. 2001); the reddening coefficient $E(B-V)$, most of them taken from isochrone fits to the clusters CMDs; and the expected distance moduli in the direction of each field. Also shown is the total number of stars found in each field. The distance moduli

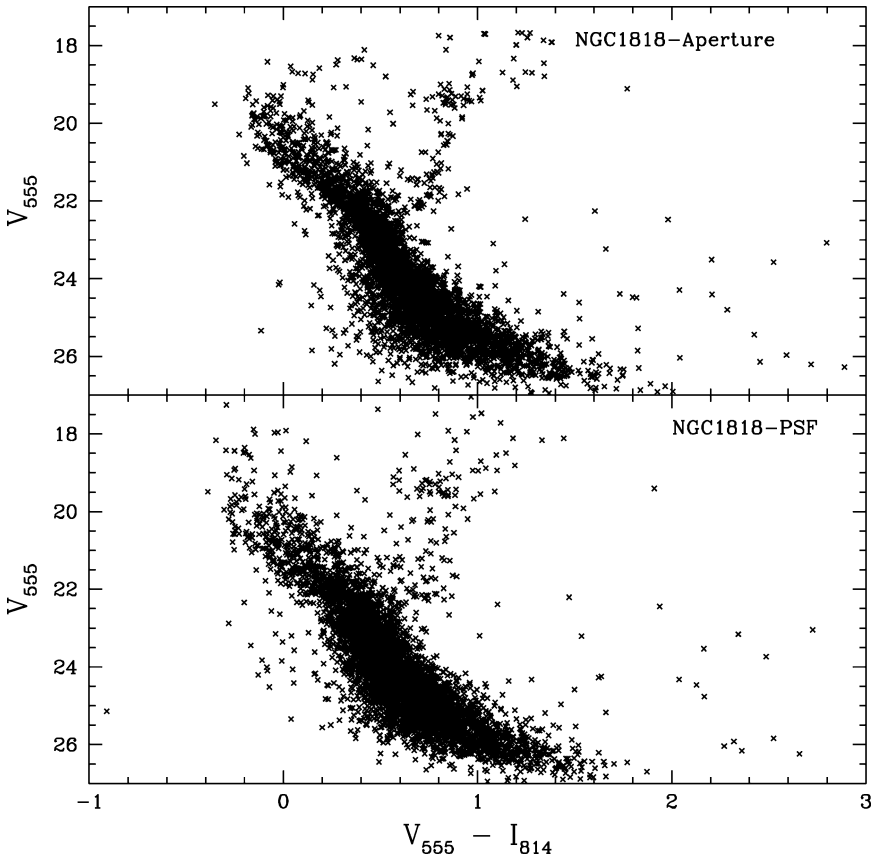

Figure 1. Comparison between the CMD built from aperture photometry (upper panel) and the one built by PSF modelling and fitting (lower panel).

were inferred assuming a disc model for the distribution of stars in the inner and intermediate regions of the LMC, with the plane of the disc inclined by 45° relative to the sky, its centre at a distance modulus of $m - M = 18.5$ (Panagia et al. 1991), the line of nodes pointing in the north–south direction and the east side of the disc lying on foreground (Westerlund 1990).

Each field is located 7.3 arcmin from the neighbouring cluster. From the table it is clear that this is well beyond the visual radii of each cluster, therefore making cluster contamination of our field stars a negligible effect, unless a substantial fraction of the original stars making up each cluster has been tidally stripped from them. We discuss this issue in the next section.

2.1 Sample selection and photometry

All exposures were put through the standard *HST* pipeline procedure that corrects them for several instrumental effects, such as bias and dark currents and flat-fielding (Holtzmann et al. 1995a). The two exposures taken in each field/filter configuration were then combined using the IRAF task CRREJ, in order to increase the signal-to-noise ratio and to remove cosmic rays.

The IRAF DAOPHOT package was used for most of the photometry. An automated search for peaks in the light distribution was carried out with the task DAOFIND. Events 5σ above the sky background (where σ is the standard deviation in the background counts) were selected. A full-width at half maximum (FWHM) of 1.4 pixel (0.14 arcsec) was adopted for point sources in the three Wide Field Camera (WFC) chips, whereas a FWHM = 2 pixels (0.1 arcsec) was used for the Planetary Camera (PC) chip. Magnitudes were obtained in two ways: using aperture photometry (with the PHOT task) and by fitting a point spread function (PSF) model to a template (built with the PSF task from bright, isolated and unsaturated stars in the images themselves) and applying it to all selected objects (ALLSTAR task).

Fig. 1 shows the CMD obtained for the same sample with each method. A 2-pixel (0.2 arcsec) aperture was used to build the upper CMD. As for the PSF fitting, we found the best-fitting Moffat function with $\beta = 1.5$ (Moffat 1969; Elson et al. 1995) to our template and applied it to all detected objects, resulting in the lower CMD in the figure. The aperture photometry data yielded narrower main-sequence and giant branches as attested by Fig. 1 and was therefore used throughout the analysis.

Sample selection and photometry were carried out independently for both filters. The final sample used in each field (the number of stars in which is listed in Table 2) resulted from a positional match of the two independently derived samples. Most spurious objects were automatically thrown out by this matching procedure. Any remaining extended sources or spurious detections

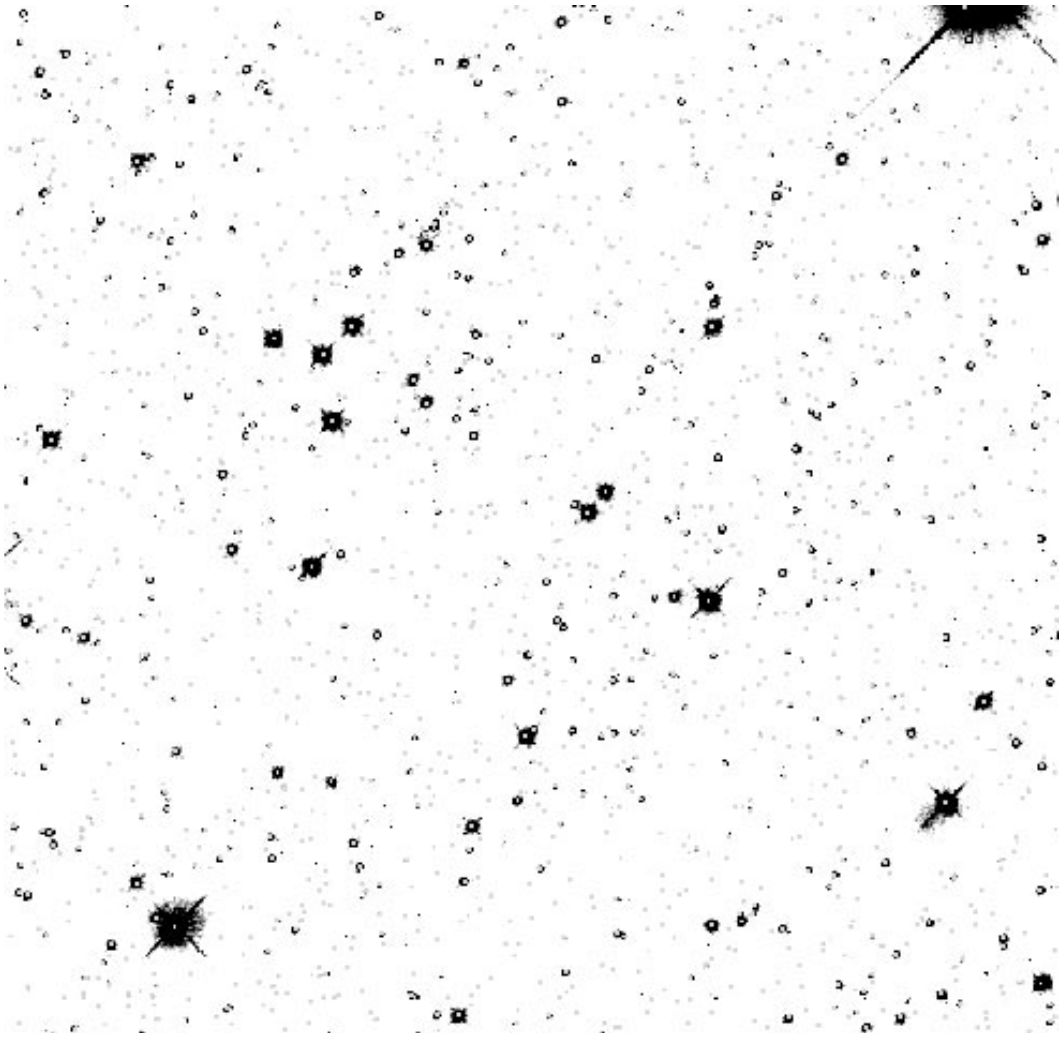

Figure 2. A sample image of our data showing LMC field stars of different magnitudes. The stars that made it into our final sample are marked with points.

(usually located along diffraction spikes of bright stars) were eliminated by eye.

In Fig. 2 we show chip 3 in the NGC1818 field imaged with the F555W filter. Dots indicate the objects remaining in our final sample. Notice the absence of non-stellar objects and the inclusion of essentially all stars visible in the figure.

Aperture magnitudes in both filters were corrected for infinite aperture. A charge transfer effect (CTE) correction was also applied to the data. Both corrections followed the prescriptions given by Holtzman et al. (1995a,b). Photometric zero-points were also taken from these references. More recently, Whitmore, Heyer & Casertano (1999) have derived more detailed CTE corrections. We tested the difference between the two correction methods for one of our fields and found at the most a 0.05-mag effect for our faintest magnitudes. As this systematic affects both filters the same way, it has a negligible effect on the $(V_{555} - I_{814})$ colours and a very small effect on our brighter magnitudes. We therefore did not redo the analysis using the more recent CTE correction by Whitmore et al. (1999).

As well as the aperture and CTE corrections, the data were also corrected for extinction and reddening using the $E(B - V)$ values listed in Table 2. The corresponding A_{555} and A_{814} values were taken from Holtzman et al. (1995b).

3 THE COLOUR–MAGNITUDE DIAGRAMS

The final CMDs for each field are shown in Figs 3 and 4. The fields are ordered with increasing angular distance from the LMC centre (see Table 1). In all panels, a clear main sequence stretches all the way down to $V_{555} \simeq 26$. The giant branch is also visible along with a turn-off around $V_{555} \simeq 22.5$. As we will see later, this corresponds to an old population ($\tau \gtrsim 10$ Gyr). The red giant clump, a signature of intermediate-age stars, is also visible at $V_{555} \sim 19$ and $V_{555} - I_{814} \sim 0.9$ in most cases. Boxes are shown in one of the panels to indicate the location where the red giant clump and the base of the old giant branch are. These stars will be used in Section 4. The faint red stars at the bottom right of the CMDs are low-luminosity M dwarfs in the Galaxy.

The red giant clump is not clearly visible in three fields: NGC2209, 1868 and 1805. The first two are the farthest from the LMC centre (5.4° and 5.9° away, respectively) and have the smallest numbers of stars. As for NGC1805, it is located in a region with a patchy distribution of dust, something known to be the case for the cluster itself. This may well be responsible for the large spread in colour seen in the giant branch and, to a minor extent, in the main sequence of this cluster. Even for the remaining fields, given the smallness of our sample of clump stars, we did not attempt to study clump morphology as has been done by other authors (Beaulieu & Sackett 1998; Piatti et al. 1999; Girardi, Mermilliod & Carraro 2000), nor did we attempt to extract ages for the intermediate populations using the magnitude difference between clump and turn-off stars (Geisler et al. 1997; Bica et al. 1998).

One distinct feature in the NGC1805 and 1818 fields is the much larger number of stars in their upper main sequence, extending up to the saturation limit ($V_{555} \simeq 18.5$). This is indicative of more

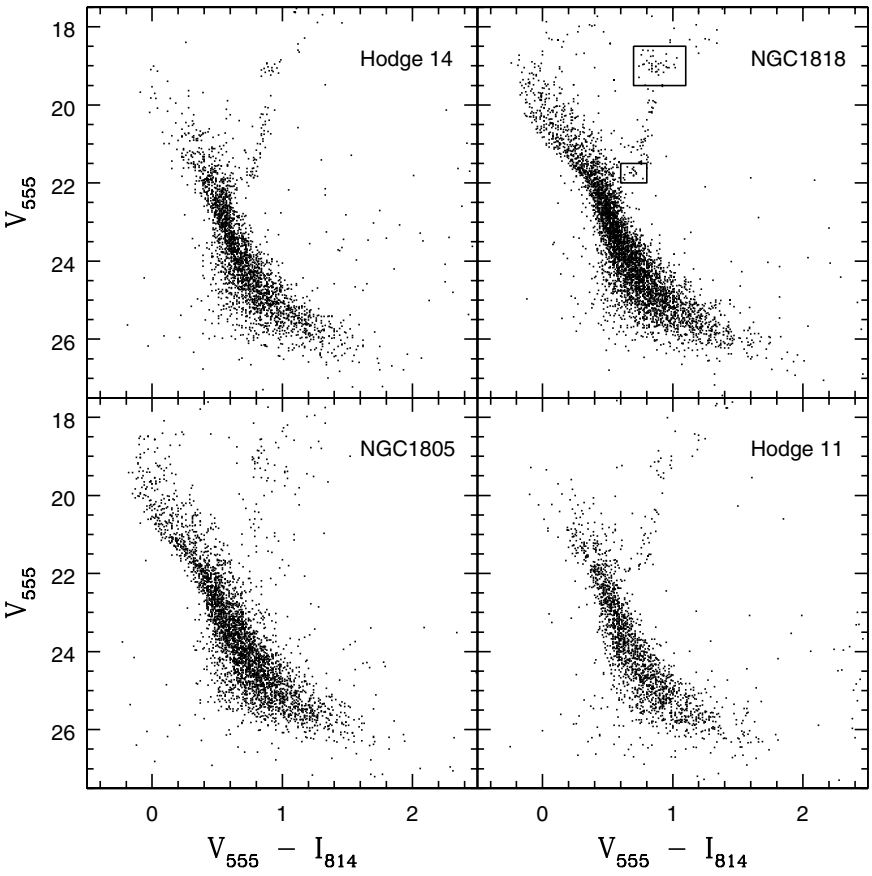

Figure 3. Final observed CMDs for four of the seven fields studied here: Hodge 14, NGC 1818, NGC 1805 and Hodge 11. The fields are ordered in increasing angular distance to the centre of the LMC. The boxes shown in the NGC1818 panel indicate the positions of the clump of red giants and of the base of the red giant branch.

recent star formation in that particular region, also attested by the young ages of the clusters themselves (Johnson et al. 2001). These fields are also the closest to the LMC bar among the seven fields studied here, there being an overall excess of stars in them as well; this excess is dominated by intermediate-age populations, as we will discuss in the next section.

In most fields, no clear turn-off is seen in their CMDs, apart from that of the older population. But in a few cases, particularly in NGC1818 and 1868, there are strong hints of an intermediate-age turn-off. As for the younger populations, we see a relative paucity of main-sequence stars brighter than $V_{555} \simeq 20$ in all fields apart from NGC1805 and 1818.

Isochrone fits were used in an attempt to derive ages and metallicities typical of the individual populations seen, especially for the oldest and relatively unstudied stellar component in the LMC. We used the Padova isochrones (Bertelli et al. 1994) for that purpose. A grid of isochrones with ages and metallicities respectively in the range $4\,\mathrm{Myr} \leq \tau \leq 16\,\mathrm{Gyr}$ and $-1.7 \leq [\mathrm{Fe/H}] \leq 0.4$ are available for CMD fitting. However, the magnitudes and colours are in the Johnson–Cousins (*UBVRI*) system, which would require us to calibrate our *HST* data. As an alternative, we used, whenever possible, the smaller set of Padova isochrones converted to the *HST* filters by Guy Worthey (private communication). We should stress, however, that the F555W and F814W filters closely match the standard *V* and *I*; the calibration terms are thus small.

Figs 5 and 6 show the same CMDs as in Figs 3 and 4 but now with a set of isochrones superposed on them. In each panel, the distance modulus listed in Table 2 was applied to the isochrones to make them consistent with the data. As mentioned before, these values of distance moduli were inferred assuming a planar distribution of LMC stars, inclined by 45° relative to the celestial sphere and with the line of nodes pointing in the North–South direction (Westerlund 1990).

In all fields available, it is possible to fit the oldest population with $10 \lesssim \tau \lesssim 16\,\mathrm{Gyr}$ isochrones with $[\mathrm{Fe/H}] = -1.7$. The only exception is NGC2209, for which a $[\mathrm{Fe/H}] = -1.3$ is required. These isochrones provide very good fits to the subgiant branches and, in most cases, account nicely for the giant branches as well. For NGC1805, given its ill-defined giant branch, the $\tau = 12.6\,\mathrm{Gyr}$ isochrone is used only for guidance.

As mentioned before, in most fields it is hard to visually identify isolated main-sequence turn-off points or subgiant branches associated with individual populations. For instance, in the two fields located in star-forming regions, NGC1805 and 1818, the upper mainsequence ($18.5 \lesssim V_{555} \lesssim 20.5$) is clearly wider than would be the case given the photometric errors alone. This is consistent with age spreads caused by continuing star formation in the past 1.5 Gyr. Despite the smaller number of stars, a similar conclusion holds for the other fields.

For NGC1868, on the other hand, a clear turn-off associated with stars of $\tau \simeq 2\,\mathrm{Gyr}$ and $[\mathrm{Fe/H}] \simeq -0.7$ is visible. A slightly older turn-off, with $\tau \simeq 3\,\mathrm{Gyr}$ and the same metallicity is apparent in NGC1818. A hint for a yet-older event of enhanced star formation is also present in the field near NGC1831 ($\tau \simeq 4.0\,\mathrm{Gyr}$).

Notice that in a couple of cases none of the isochrones used fit

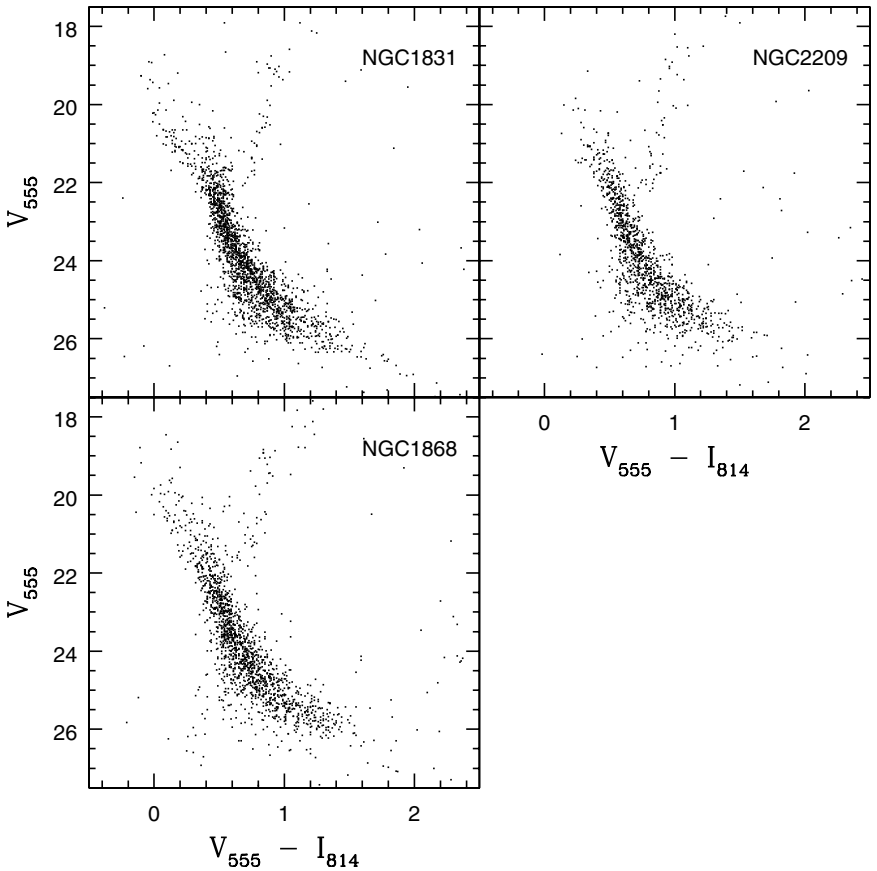

Figure 4. Final observed CMDs for three of the seven fields studied here: NGC 1831, 2209 and 1868. The fields are ordered in increasing angular distance to the centre of the LMC.

the lower main sequence adequately. The clearest such case is Hodge 11, where the isochrones are too red compared to the bulk of the stars. This is indicative of lower metallicities, larger distance moduli or a combination of both.

One possible problem with the CMDs studied here is contamination by cluster stars. Except for NGC 1805 and 1818, the clusters located near our fields are old enough so that stars at typical escape velocities from them would have time to cover the angular distance to our fields. We note, however, that the density profiles of these rich clusters flatten out considerably within our WFPC2 fields centred on them, usually reaching number densities of the order of a few per cent of the central cluster density at distances of about 20 pc from the centre (Santiago et al. 2001). In an attempt to assess contamination of our field stars by cluster stars, we compared the surface brightness values, μ_{555}, in our fields with those shown in Santiago et al. (2001). Our μ_{555} values for each field are listed in Table 3. We show the μ_{555} values over the entire field (column 2) as well as that for each WFC chip separately (columns 3, 4 and 5). We choose surface brightness rather than number density of stars as a means of comparison because the former is less sensitive to exposure time. In three fields, these values are extremely close to those in the outermost radial bin shown in Santiago et al. (2001) (last column of Table 3). For the field close to NGC 1818, μ_{555} is actually brighter by 0.5 mag than in the outermost radius in the cluster field. It is hard to explain this by any effect other than real variations in the surface brightness of field stars; such variations are also attested to on a smaller scale by the chip-to-chip scatter seen in the Table. The two cases where the field is fainter than the 'cluster outer radius', H14 and NGC 1831, could signal cluster contamination. Notice, however, that the discrepancies may also be accounted for by field-to-field scatter. Therefore, unless escaping cluster stars make up a roughly uniform-density halo stretching out to $\simeq 100$ pc from the centres of the clusters, our surface brightness comparisons rule out strong cluster contamination in most of our fields.

4 LUMINOSITY FUNCTIONS AND DENSITY PROFILES

In this section we extract and compare the luminosity functions (LFs) of main-sequence stars below the turn-off point of the oldest population. In this region of the CMD, main-sequence stars belonging to the different populations found in each field are mixed up. Their composite LFs can then be expressed as

$$\Phi(M_{555})\,\mathrm{d}M_{555} = \sum_{i}^{N_\mathrm{p}} f_i \psi_i[m(M_{555})] \left(\frac{\mathrm{d}m}{\mathrm{d}M_{555}}\right)_i \mathrm{d}M_{555}, \qquad (1)$$

where $\Phi(M_{555})$ is the differential LF, written as a function of the absolute magnitude in the $F555W$ filter, $\psi_i(m)$ is the differential mass function of the i^{th} population and N_p is the number of populations present, each one contributing a fraction f_i to the total number of stars in the field. The stellar mass corresponding to a specific value of M_{555} will vary from one population to another, depending on the mass–luminosity relation and its derivative, usually a function of metallicity.

Thus, assuming that the same stellar populations contribute to all fields, variations in the composite LF shown in equation (1) will

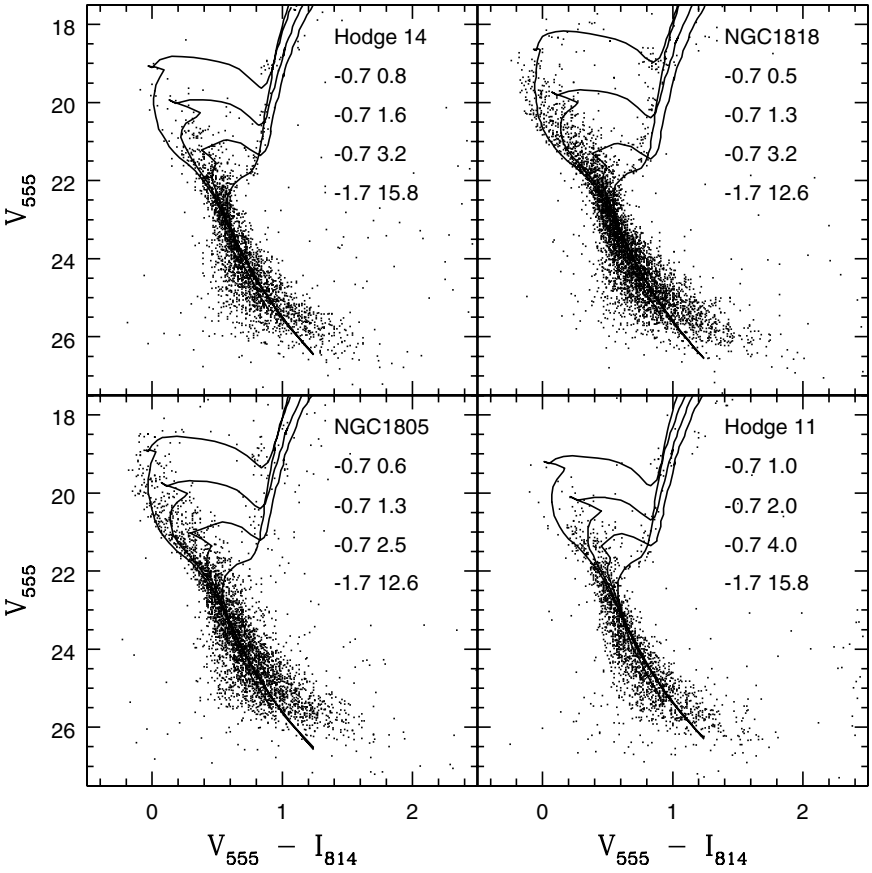

Figure 5. Isochrone fits to the observed CMDs for Hodge 14, NGC 1818, NGC 1805 and Hodge 11. Metallicities and ages are indicated in each panel, in the first and second columns, respectively, by the [Fe/H] and τ (in Gyr) values.

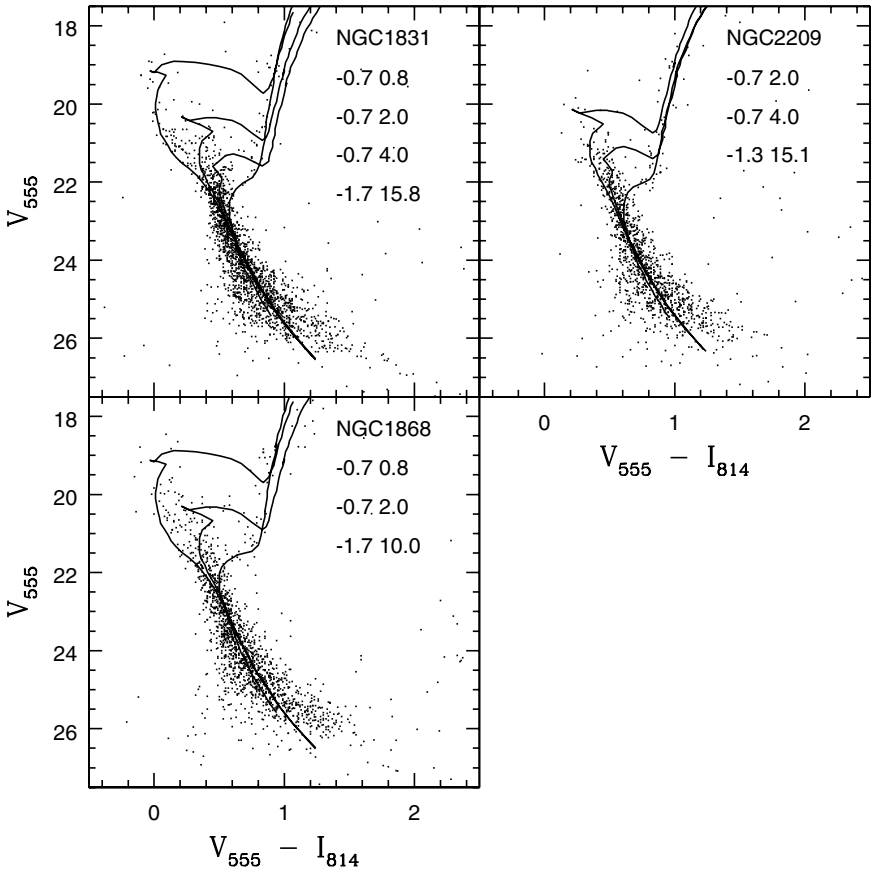

Figure 6. Isochrone fits to the observed CMDs for NGC 1831, 2209 and 1868. Metallicities and ages are indicated in each panel, in the first and second columns, respectively, by the [Fe/H] and τ (in Gyr) values.

Table 3. Surface brightness values (in mag arcsec^{-2}) for the WFPC2 fields in this paper (columns 2 thru 5; 7.3 arcmin away from the clusters) and for the outermost radius (6th column; ~ 1.7 arcmin) of the profiles shown by Santiago et al. 2001.

Name	Field	WF2	WF3	WF4	Cluster
Hodge 14	24.4	24.4	24.5	24.2	23.7
NGC1805	23.5	23.6	23.5	23.6	23.6
NGC1818	23.1	22.9	23.2	23.2	23.6
NGC1831	24.7	25.0	24.6	24.6	23.7
NGC1868	24.7	24.6	24.8	24.7	24.8
NGC2209	25.1	25.0	25.1	25.2	25.0

depend only on the relative contribution to the total number of stars given by each population, which is quantified by the fractions f_i.

The LFs, normalized to unity, are shown in Fig. 7, in the range $4 < M_{555} < 6.5$. We divided the figure into two panels to avoid cluttering. In the range considered, V_{555} is typically $\lesssim$24.5, making completeness corrections unimportant, given that our *HST* fields are not very crowded.

A visual inspection shows that the LF shapes are similar to one another. The field star LF close to Hodge 14 looks slightly steeper than the others shown in the upper panel, whereas that of NGC1818 seems shallower. In order to quantify any discrepancy among the field LFs, we ran the Kolmogorov–Smirnov test (KS test) for all pairs of LFs. The probabilities that the LFs in each pair are derived from the same parent distribution of stars is listed in Table 4.

The probabilities are very large in most cases and in all of them

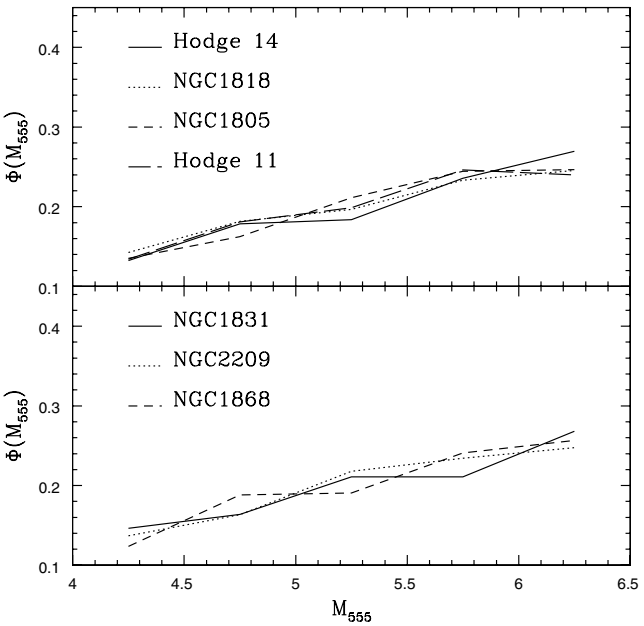

Figure 7. Luminosity functions of lower main-sequence stars for the different fields as indicated.

$P \geq 10$ per cent. We thus conclude that, under the assumptions outlined in the beginning of this section, the mixture in stellar populations does not vary significantly from one field to another. Notice, however, that this statement is restricted to a narrow

Table 4. KS test probabilities obtained by comparing pairs of LFs.

Field pairs	Probability (P)
Hodge 11, Hodge 14	0.45
Hodge 11, NGC1805	0.88
Hodge 11, NGC1818	0.85
Hodge 11, NGC1831	0.66
Hodge 11, NGC1868	0.88
Hodge 11, NGC2209	0.95
Hodge 14, NGC1805	0.45
Hodge 14, NGC1818	0.28
Hodge 14, NGC1831	0.42
Hodge 14, NGC1868	0.78
Hodge 14, NGC2209	0.77
NGC1805, NGC1818	0.10
NGC1805, NGC1831	0.73
NGC1805, NGC1868	0.91
NGC1805, NGC2209	0.91
NGC1818, NGC1831	0.73
NGC1818, NGC1868	0.49
NGC1818, NGC2209	0.58
NGC1831, NGC1868	0.71
NGC1831, NGC2209	0.86
NGC1868, NGC2209	0.91

Table 5. KS results for simulated composite LFs with different mixtures of intermediate-age and old stars.

d_1	d_2	P(25%)	P(50%)	P(75%)
20–80	80–20	4.3E−5	6.7E−4	5.6E−3
30–70	70–30	4.0E−3	0.034	0.086
40–60	60–40	0.080	0.253	0.455
50–50	50–50	0.208	0.455	0.687

interval in luminosity and mass and assumes that the same populations are present in all fields. This latter assumption is probably true, considering that most LMC stars are older than the typical crossing time in the central 10 kpc of that galaxy.

One important issue is how sensitive the KS test is to variations in population mix among the fields. This may be especially important when the LFs available for comparison cover a narrow mass range, as in our case. In order to assess the sensitivity of our composite LFs, we have created and compared artificial LFs with variable contributions from two different populations: one markedly old and metal-poor ($\tau = 12.6$ Gyr; [Fe/H] $= -1.7$) and the other of intermediate age ($\tau = 2$ Gyr; [Fe/H] $= -0.7$). This choice is consistent with our isochrone fits shown in the previous section and with the evidence for an age gap in the LMC star formation. The results of such artificial simulations are shown in Table 5. The first two columns show the population mixture used to create the two composite LFs (d_1 and d_2) to be compared; the first (second) number in each column gives the percentage of stars from the old (intermediate) population. Notice that we always compare two composite LFs where the percentage values of population mix are swapped. In building these composite LFs, we assumed that both populations have a Salpeter initial mass function. The last three columns in Table 5 show the 25 per cent, median and 75 per cent positions of the distribution of KS probabilities over 100 realizations. As expected, the KS P values are large when the two populations contribute similar fractions ($\gtrsim$40 per cent); when we compare composite LFs for which each population in turn contributes about 2/3 of the stars or more, the probabilities become smaller than those in Table 4. Thus, we conclude that the KS test is capable of ruling out variations larger than about 30 per cent in population mix from one field to another.

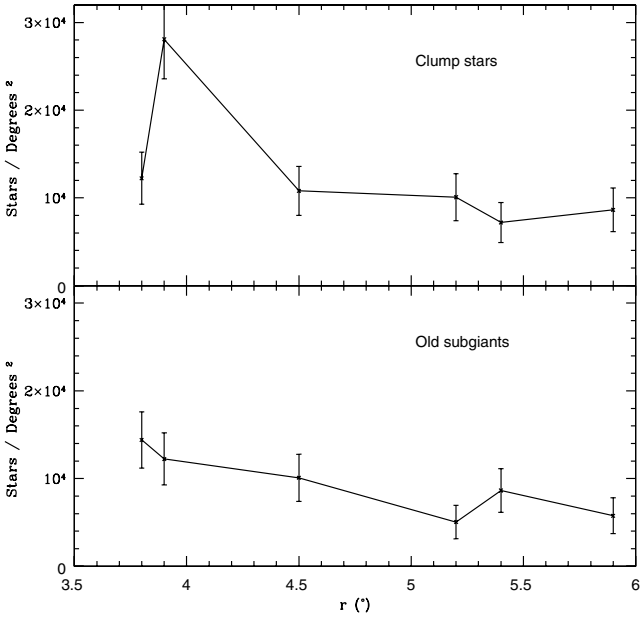

Figure 8. Density profiles. Upper panel: red giant clump. Lower panel: old subgiants.

We next attempt to isolate stars belonging to old and intermediate-age populations in order to infer their distribution within the LMC. Our fields are located from about 4° to 6° from the centre of the LMC. In Fig. 8 we show the surface density of stars of intermediate (upper panel) and old (lower panel) populations, both scaled to a 1 deg^2 solid angle.

The intermediate-age stars were extracted from the red giant clump position. All stars contained in a box centred on $(V_{555}, V_{555} - I_{814}) = (19, 0.9)$ and with $\Delta V_{555} = 1$ mag and $\Delta(V_{555} - I_{814}) = 0.4$ were counted and considered to be of an intermediate age ($0.5 \lesssim \tau \lesssim 10$ Gyr; Hatzidimitriou & Hawkins 1989). A similar procedure was used for the old stars: a box with $\Delta V_{555} = 0.5$ mag and $\Delta(V_{555} - I_{814}) = 0.2$ was placed at the base of the giant branch, redwards of the old main-sequence turn-off at $V_{555} \simeq 22.5$, where only the evolved stars belonging to an old $\tau \gtrsim 10$ Gyr reside. These boxes are the ones shown in one of the panels in Fig. 3.

A large peak in the position corresponding to the field close to NGC1818, $r = 3.9°$, is seen in Fig. 8. As mentioned earlier, this is, along with the one near NGC1805, the closest field to the LMC bar, where intermediate-age stars are known to dominate (Gallagher et al. 1996; Elson et al. 1997). As for the field close to NGC1805, it was not possible to derive old and intermediate stars counts from its ill-defined clump and giant branch.

Santos et al. (1999) also show a number density profile of clump stars based on a large-angle ground-based sample in the outer LMC. Apart from the large peak in NGC 1818, there is excellent agreement between both profiles within the angular range in common. If we again disregard the field close to NGC 1818, our two profiles are similar, with the number of old stars declining slightly more steeply than the number of intermediate age ones. These two profiles are representative of regions situated well away from the bar and/or star-forming regions.

5 SUMMARY AND CONCLUSIONS

We have obtained and analysed seven deep $V \times (V - I)$ CMDs ($V_{555} \lesssim 26$) of field stars in the LMC using *HST* WFPC2. Our WFPC2 fields, located from 4° to 6° from the LMC centre and within $\simeq 7$ arcmin from rich star clusters, contain from 1300 to 5000 stars each. The CMDs show clear evidence of an old stellar population with $\tau \gtrsim 10^{10}$ Gyr and [Fe/H] $\lesssim -1.7$. Red giant clumps are visible in most CMDs as are main sequences extending up to $V_{555} \simeq 20$, indicative of stars with intermediate ages ($\tau \gtrsim 1$–1.5 Gyr). Younger field stars are clearly seen only in the fields close to NGC 1805 and 1818.

The CMDs suggest a complex star formation process in the LMC, especially in the last $\sim$2.0 Gyr. A wide upper main sequence, much wider than expected from photometric errors alone, reveals a continuous spread in the ages of field stars younger than $\tau \simeq$ 2.0 Gyr around NGC 1805 and 1818. As for older populations, we have CMDs both with and without discrete main-sequence turn-offs in the range $2 \lesssim \tau \lesssim 4$ Gyr. Events of enhanced star formation within this range of ages are visible in the fields close to NGC 1868, 1818 and 1831. It is interesting to note that these fields are all in the same direction (north to north-west) relative to the LMC bar. The other CMDs show at best only hints of individual intermediate populations. A hint of a similar east–west difference in stellar populations in the LMC had been detected by Vallenari et al. (1996). The old populations are also found to have variable ages as inferred from isochrone fits.

We analysed the shapes of the luminosity functions in the lower part of the CMDs, where the different populations are combined, in order to search for possible significant differences in population mix. The field-star luminosity functions look remarkably similar, both visually and according to the KS test. Our results indicate that variations larger than 30 per cent in population mix from one field to another are unlikely, since they would probably translate into significant differences in the composite LFs.

Finally, we estimated the surface density of stars of intermediate and old ages in each field, by counting stars in regions of the CMD occupied by a single population. The angular density profile of $\tau \gtrsim 10^{10}$ stars is slightly steeper than that of intermediate-age ones.

We should point out that the current sample is being enlarged by deeper *HST* WFPC2 fields close to the ones studied here. This larger data set, along with two-dimensional modelling of the CMDs and use of modern statistical methods (Saha 1998; Valls-Gabaud & Lastennet 1999; Hernandez, Valls-Gabaud & Gilmore 1999; Kerber, Javiel & Santiago 2001) will provide a more detailed picture of the field-star formation history in the LMC.

ACKNOWLEDGMENTS

The authors are very grateful to Rebecca Elson for her strong and very positive influence during her last years among us. This work was partially supported by CNPq and PRONEX/FINEP 76.97.1003.00.

REFERENCES

Beaulieu J., Sackett P., 1998, AJ, 116, 209
Beaulieu S. F., Elson R., Gilmore G., Johnson R., Tanvir N., Santiago B., 1998, in Chu Y.-H., Suntzeff N. B., Hesser J. E., Bohlender D. A., eds, Proc. IAU Symp. 190, New Views of the Magellanic Clouds. Astron. Soc. Pac., San Francisco, p. 460
Bertelli G., Mateo M., Chiosi C., Bressan A., 1992, ApJ, 388, 400
Bertelli G., Bressan A., Chiosi C., Fagotto F., Nasi E., 1994, A&AS, 106, 275
Bica E., Geisler D., Dottori H., Clariá J., Piatti A., Santos J., 1998, AJ, 116, 723
Da Costa G. S., 1991, AJ, 100, 162; in The Magellanic Clouds, IAU Symposium 148, edited by R. Haynes and D. Milne (Kluwer, Dordrecht), p. 183
Elson R. A. W., Gilmore G. F., Santiago B. X., Casertano S., 1995, AJ, 110, 682
Elson R. A. W., Gilmore G. F., Santiago B. X., 1997, MNRAS, 289, 157
Elson R., Gilmore G., Aarseth S., Davies M., Sigurdsson S., Santiago B., Hurley J., 1998a, in Richtler T., Braun J. M., eds, Proc. Bonn/Bochum-Graduiertenkolleg Workshop, The Magellanic Clouds and Other Dwarf Galaxies. Shaker Verlag, Aachen, p. 243
Elson R., Tanvir N., Gilmore G., Johnson R., Beaulieu S., 1998b, in Chu Y.-H., Suntzeff N. B., Hesser J. E., Bohlender D. A., eds, Proc. IAU Symp. 190, New Views of the Magellanic Clouds. Astron. Soc. Pac., San Francisco, p. 417
Gallagher et al., 1996, ApJ, 466, 732
Geha M. C. et al., 1998, AJ, 115, 1045
Geisler D., Bica E., Dottori H., Clariá J., Piatti A., Santos J., 1997, AJ, 114, 1920
Girardi L., Mermilliod J.-C., Carraro G., 2000, A&A, 354, 892
Hatzidimitriou D., Hawkins M. R. S., 1989, MNRAS, 241, 667
Hernandez X., Valls-Gabaud D., Gilmore G., 1999, MNRAS, 304, 705
Holtzman J. A., Burrows C. J., Casertano S., Hester J. J., Trauger J. T., Watson A. M., Worthey G., 1995a, PASP, 107, 1065
Holtzman J. A. et al., 1995b, PASP, 107, 156
Holtzman J. A. et al., 1997, AJ, 113, 656
Jensen J., Mould J., Reid N., 1988, ApJS, 67, 77
Johnson R., Elson R., Gilmore G., Beaulieu S., Tanvir N., 1998, in Freudling W., Hook R., eds, ESO Conf. and Workshop Proc. 55, NICMOS and the VLT: A New Era of High Resolution Near Infrared Imaging and Spectroscopy. Pula, Sardinia, Italy
Johnson R., Beaulieu S. F., Gilmore G. F., Hurley J., Santiago B., Tanvir N., Elson R., 2001, MNRAS, 324, 367
Kerber L. O., Javiel S. C., Santiago B. X., 2001, A&A, 365, 424
Moffat A., 1969, A&A, 3, 455
Olszewski E. W., 1993, in Smith G., Brodie J., eds, ASP Conf. Ser. Vol. 48, The Globular Cluster-Galaxy Connection. Astron. Soc. Pac., San Francisco, p. 351
Olszewski E. W., Suntzeff N. B., Mateo M., 1996, ARA&A, 34, 511
Panagia N., Gilmozzi R., Macchetto F., Adorf H.-M., Kirshner R. P., 1991, ApJ, 380, L23
Piatti A., Geisler D., Bica E., Clariá J., Santos J., Sarajedini A., Dottori H., 1999, AJ, 118, 2865
Saha P., 1998, MNRAS, 115, 1206
Santiago B., Beaulieu S., Johnson R. A., Gilmore G., 2001, A&A, 369, 74
Santos J., Piatti A., Clariá J., Bica E., Geisler D., Dottori H., 1999, AJ, 117, 2841
Schommer R. A., Olszewski E. W., Suntzeff N. B., Harris H. C., 1992, AJ, 103, 447
Vallenari A., Chiosi C., Bertelli G., Ortolani S., 1996, A&A, 309, 358
Valls-Gabaud D., Lastennet E., 1999, Rev. Mex. Astron. Astrofis., Ser. Conf., 8, 111
Westerlund B. E., 1990, A&AR, 2, 29
Westerlund B. E., Linde P., Lynga G., 1995, A&A, 298, 39
Whitmore B., Heyer I., Casertano S., 1999, PASP, 111, 1559

This paper has been typeset from a TEX/LATEX file prepared by the author.